Magnification of the spin Hall effect in a bilayer electron gas

Pei-Qing Jin and You-Quan Li
Zhejiang Institute of Modern Physics and Department of Physics, Zhejiang University, Hangzhou 310027, People's Republic of China
(Received 6 May 2007; published 13 December 2007)

Spin transport properties of a coupled bilayer electron gas with Rashba spin-orbit coupling are studied. The definition of the spin currents in each layer as well as the corresponding continuitylike equations in the bilayer system are given. The curves of the spin Hall conductivities obtained in each layer exhibit sharp cusps around a particular value of the tunneling strength and the conductivities undergo sign changes across this point. Our investigation on the impurity effect manifests that an arbitrarily small concentration of nonmagnetic impurities does not suppress the spin Hall conductivity to zero in the bilayer system. Based on these features, an experimental scheme is suggested to detect a magnification of the spin Hall effect.

DOI: 10.1103/PhysRevB.76.235311 PACS number(s): 72.25.−b, 72.10.−d, 03.65.−w

I. INTRODUCTION

Manipulating the spin degree of freedom for electrons has recently brought in an emerging information technology, spintronics,[1–3] which offers clues for designing devices based on traditional materials with spin-related effects. In this promising field, the spin Hall effect[4–6] is regarded as a candidate method to inject spin current in semiconductors. Based on the spin-orbit coupling (SOC), an external electric field is required to drive a transverse spin current while the magnetic field is not necessary, which is much different from the traditional applications of the spin degree of freedom. A universal spin Hall conductivity $e/8\pi$ is predicted theoretically in a clean single layer electron system.[6] Several groups' calculations[7–11] showed that nonmagnetic impurities would suppress this spin Hall conductivity to zero, while others indicated that the spin Hall conductivity is not zero in the presence of magnetic impurities.[12,13] Experimentally, the spin accumulation in nonmagnetic semiconductors has been observed[14,15] and the spin current was detected either by Kerr rotation microscopy[16] or by two-color optical coherence control techniques.[17] Very recently, a direct electronic measurement of the spin Hall effect has been reported[18] where the spin current induces the charge imbalance and a voltage is detected.

As the SOC, which is crucial to the spin Hall effect, is a relativistic effect and thus comparably weak, a natural question is how to strengthen this effect. In the light of single layer systems being considered in current literature, one may ask whether a multilayer system possesses a magnification effect and what new phenomena will take place if the tunneling between layers is taken into account. Another more realistic question is what will happen if there exist impurities in a multilayer system.

In this paper, we investigate the spin transport properties in a coupled bilayer electron system with different SOC strength in each layer as well as the tunneling between layers. As a starting point, we generalize the definitions of spin currents to a coupled bilayer system and obtain the corresponding "continuitylike" equations. Carrying out calculations of the spin current in the Heisenberg representation, we find that the spin Hall conductivity in each layer manifests abrupt enhancement around a particular value of the tunneling strength between layers and undergoes a sign change across this point. The influence of impurities is also studied. We indicate that the spin Hall conductivity in the bilayer system cannot be suppressed to zero by an arbitrarily small concentration of impurities. An experimental scheme is designed on the basis of these features to magnify the spin Hall effect near the turning point. Besides, possible logical gates are expected to be elaborated based on the sign change of the spin current across this point.

The whole paper is organized as follows. In Sec. II, we generalize the definition of the spin current in each layer and obtain the continuitylike equations. In Sec. III, the spin current as well as the spin Hall conductivity in each layer are calculated in Heisenberg representation. In Sec. IV, the influence of disorderly distributed nonmagnetic impurities on the spin Hall conductivity is investigated. In Sec. V, we show the greatly enhanced spin currents near the turning point and scheme out possible experiment to detect a magnification of the spin Hall effect. Finally, a brief summary is given in Sec. VI and some concrete expressions are written out in the Appendix.

II. CONTINUITYLIKE EQUATIONS

As a proposition to study the spin transport, we first introduce the definition of the spin current in a coupled bilayer system in this section. Throughout the whole paper, we consider a coupled bilayer system where the strength of the Rashba-type SOC in each layer are different and the tunneling between layers always occurs. The spaces spanning the electrons' spin states and layer occupations, respectively, carry out SU(2) representations. If the spin and layer representations are denoted by Pauli matrices σ_a and τ matrices τ_a, respectively, the total Hamiltonian of such a system can be written as

$$H_0 = \frac{\hbar^2 k^2}{2m} + \begin{pmatrix} \alpha_1 & 0 \\ 0 & \alpha_2 \end{pmatrix} \otimes (k_y\sigma_x - k_x\sigma_y) + \begin{pmatrix} 0 & \beta \\ \beta & 0 \end{pmatrix} \otimes I$$
$$= \frac{\hbar^2 k^2}{2m} + (\alpha_+ I + \alpha_- \tau_z) \otimes (k_y\sigma_x - k_x\sigma_y) + \beta\tau_x \otimes I, \quad (1)$$

where α_1 and α_2 refer to SOC strength in the front and back layers, correspondingly, and β the tunneling strength be-

tween layers. I stands for the unit matrix. For convenience, $\alpha_+=(\alpha_1+\alpha_2)/2$ and $\alpha_-=(\alpha_1-\alpha_2)/2$ are introduced in the second line of the above equation. Hereafter, indices a and i run from 1 to 3. Let $\psi_f=(\phi_{f\uparrow},\phi_{f\downarrow})^T$ and $\psi_b=(\phi_{b\uparrow},\phi_{b\downarrow})^T$ represent the spin states of the electrons in the front and back layers, respectively. Hereafter, the layer-index f or b labels either the front or back layer. Then a four-component wave function, denoted by $\Psi=(\phi_{f\uparrow},\phi_{f\downarrow},\phi_{b\uparrow},\phi_{b\downarrow})^T=(\psi_f,\psi_b)^T$ must be introduced for a complete quantum mechanical description of the system.

The well accepted definitions of the spin density and the spin current density in a single-layer system are $S^a=\Psi^\dagger s^a\Psi$ and $\mathbf{J}^a=\mathrm{Re}\,\Psi^\dagger\hat{\mathbf{j}}^a\Psi$, respectively. Here $s^a=\sigma_a\hbar/2$ is the spin operator and $\hat{\mathbf{j}}^a=\frac{1}{2}\{\hat{\mathbf{v}},s^a\}$ the spin current operator with the curly brackets denoting the anticommutator and $\hat{\mathbf{v}}=\frac{1}{i\hbar}[\hat{\mathbf{r}},H_0]$ the velocity operator. The boldface manifests that the quantity is a vector in the spatial space, e.g., $\mathbf{J}^a=(J_x^a,J_y^a,J_z^a)$. It is natural to define the full spin current operator for the whole bilayer system as

$$\hat{\mathbf{j}}^a=\frac{1}{2}\{\hat{\mathbf{v}},I\otimes s^a\}\equiv\begin{pmatrix}\hat{\mathbf{j}}_f^a & 0\\ 0 & \hat{\mathbf{j}}_b^a\end{pmatrix},\tag{2}$$

with $\hat{\mathbf{j}}_f^a$ and $\hat{\mathbf{j}}_b^a$ being the spin current operators in the corresponding layers. Even though the tunneling couples two layers, the spin current operator is in a block diagonal form since the tunneling is momentum independent. Then we have the spin density and the spin current density in each layer

$$S_\ell^a=\psi_\ell^\dagger s^a\psi_\ell,\quad \mathbf{J}_\ell^a=\mathrm{Re}\,\psi_\ell^\dagger\hat{\mathbf{j}}_\ell^a\psi_\ell,\tag{3}$$

where ℓ stands for f or b.

It is obvious that the presence of the SOC, which can be regarded as certain SU(2) gauge potentials $\vec{\mathcal{A}}_i$ and $\vec{\mathcal{A}}_0$,[19] leads to the nonconservation of the spin density. Hereafter, a vector in the spin space is denoted by an overhead arrow, e.g., $\vec{S}=(S^x,S^y,S^z)$. In terms of these gauge potentials, the partially conserved spin current takes a covariant form[19] and obeys the continuitylike equation, namely, $\left(\frac{\partial}{\partial t}-\eta\vec{\mathcal{A}}_0\times\right)\vec{S}+\left(\frac{\partial}{\partial x_i}+\eta\vec{\mathcal{A}}_i\times\right)\vec{J}_i=0$. Through an analogous procedure as in Ref. 19, we can derive a general continuitylike equation for the spin density in each single layer in the presence of SU(2) gauge potentials:

$$\left(\frac{\partial}{\partial t}-\eta\vec{\mathcal{A}}_{f0}\times\right)\vec{S}_f+\left(\frac{\partial}{\partial x_i}+\eta\vec{\mathcal{A}}_{fi}\times\right)\vec{J}_{fi}=\frac{i\beta}{\hbar}(\psi_b^\dagger\vec{s}\psi_f-\psi_f^\dagger\vec{s}\psi_b),$$

$$\left(\frac{\partial}{\partial t}-\eta\vec{\mathcal{A}}_{b0}\times\right)\vec{S}_b+\left(\frac{\partial}{\partial x_i}+\eta\vec{\mathcal{A}}_{bi}\times\right)\vec{J}_{bi}=\frac{i\beta}{\hbar}(\psi_f^\dagger\vec{s}\psi_b-\psi_b^\dagger\vec{s}\psi_f).\tag{4}$$

In the coupled bilayer electron gas with Rashba SOC, $\vec{\mathcal{A}}_{fx}=\frac{2m}{\eta^2}(0,\alpha_1,0)$, $\vec{\mathcal{A}}_{fy}=-\frac{2m}{\eta^2}(\alpha_1,0,0)$, $\vec{\mathcal{A}}_{bx}=\frac{2m}{\eta^2}(0,\alpha_2,0)$, $\vec{\mathcal{A}}_{by}=-\frac{2m}{\eta^2}(\alpha_2,0,0)$, and $\vec{\mathcal{A}}_{fz}=\vec{\mathcal{A}}_{f0}=\vec{\mathcal{A}}_{bz}=\vec{\mathcal{A}}_{b0}=0$ with $\eta=\hbar$. The tunneling between layers gives rise to the term on the right hand side of Eq. (4) and this term results in additional nonconservations for the spin density in each layer.

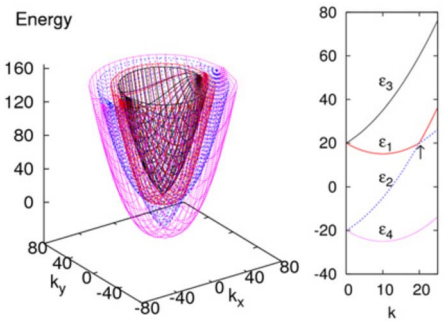

FIG. 1. (Color online) The four energy bands corresponding to the four eigenstates given in Eq. (6). The surface of revolution in the left panel is obtained by revolving the curves in the right panel with respect to the vertical axis. The ↑ in the right panel marks the level crossing point of ε_1 and ε_2.

III. SPIN CURRENTS IN A CLEAN SYSTEM

In this section, we calculate the spin currents for a clear system in Heisenberg representation.[20] A weak electric field $\mathbf{E}=E\hat{x}$ applied on both layers is regarded as a perturbation. We mainly focus on $J_{\ell y}^z$ component of the spin current in the ℓ layer, which is flowing perpendicularly to the electric field with the spin polarized in the z direction.

Diagonalizing the unperturbed Hamiltonian (1), we obtain four energy bands:

$$\varepsilon_1=\frac{\hbar^2k^2}{2m}+(\sqrt{\beta^2+\alpha_-^2k^2}-\alpha_+k)\mathrm{sgn}(k_t-k),$$

$$\varepsilon_2=\frac{\hbar^2k^2}{2m}-(\sqrt{\beta^2+\alpha_-^2k^2}-\alpha_+k)\mathrm{sgn}(k_t-k),$$

$$\varepsilon_3=\frac{\hbar^2k^2}{2m}+\sqrt{\beta^2+\alpha_-^2k^2}+\alpha_+k,$$

$$\varepsilon_4=\frac{\hbar^2k^2}{2m}-\sqrt{\beta^2+\alpha_-^2k^2}-\alpha_+k,\tag{5}$$

with

$$\mathrm{sgn}(x)=\begin{cases}1 & \text{if } x>0\\ 0 & \text{if } x=0\\ -1 & \text{if } x<0,\end{cases}$$

and $k_t=\beta/\sqrt{\alpha_+^2-\alpha_-^2}$ denoting a special point where $\varepsilon_1=\varepsilon_2=\hbar^2k_t^2/2m$. The landscapes of these bands are plotted in Fig. 1, in which ↑ in the right panel marks the level crossing point of ε_1 and ε_2 at k_t. As we will see later, the spin Hall conductivity exhibits sharp cusps around this point. In the following, we consider the case $k<k_t$ which has the same result as $k>k_t$. The eigenvectors $\Psi_j=(\psi_{fj},\psi_{bj})^T$ with $j=1,2,3,4$ labeling the band indices are given by

$$\Psi_1 = N_1 \begin{pmatrix} ie^{-i\varphi}(\alpha\_k - \sqrt{\beta^2 + \alpha\_^2 k^2}) \\ -(\alpha\_k - \sqrt{\beta^2 + \alpha\_^2 k^2}) \\ -ie^{-i\varphi}\beta \\ \beta \end{pmatrix},$$

$$\Psi_2 = N_2 \begin{pmatrix} ie^{-i\varphi}(\alpha\_k - \sqrt{\beta^2 + \alpha\_^2 k^2}) \\ (\alpha\_k - \sqrt{\beta^2 + \alpha\_^2 k^2}) \\ ie^{-i\varphi}\beta \\ \beta \end{pmatrix},$$

$$\Psi_3 = N_3 \begin{pmatrix} ie^{-i\varphi}(\alpha\_k + \sqrt{\beta^2 + \alpha\_^2 k^2}) \\ (\alpha\_k + \sqrt{\beta^2 + \alpha\_^2 k^2}) \\ ie^{-i\varphi}\beta \\ \beta \end{pmatrix},$$

$$\Psi_4 = N_4 \begin{pmatrix} ie^{-i\varphi}(\alpha\_k + \sqrt{\beta^2 + \alpha\_^2 k^2}) \\ -(\alpha\_k + \sqrt{\beta^2 + \alpha\_^2 k^2}) \\ -ie^{-i\varphi}\beta \\ \beta \end{pmatrix}, \quad (6)$$

where $\varphi = \tan^{-1}(k_y/k_x)$ and the normalization coefficients N_j are given in the Appendix.

The spin current operator for the whole bilayer system is given by $\hat{j}_y^z = \frac{1}{2}\{\hat{v}_y, I \otimes s^a\} = \frac{\hbar^2 k_y}{2m} I \otimes \sigma_z$. Time evolutions of operators are governed by Heisenberg equation of motion. Thus, we have $k_x = k_{0x} - \frac{eEt}{\hbar}$ and $k_y = k_{0y}$ with k_{0x} and k_{0y} being the initial values and

$$\frac{\partial}{\partial t}(I \otimes \sigma_z) = \frac{2}{\hbar}[\alpha_+ k_x I \otimes \sigma_x + \alpha_+ k_y I \otimes \sigma_y + \alpha\_ k_x \tau_z \otimes \sigma_x + \alpha\_ k_y \tau_z \otimes \sigma_y]. \quad (7)$$

Obviously, the time evolution of $I \otimes \sigma_z$ depends on those of other four-by-four Hermitian matrices, such as $I \otimes \sigma_x$ which also depends on other matrices. Hence, we need to deal with the time evolutions of 16 matrices $\{I \otimes I, I \otimes \sigma_x, I \otimes \sigma_y, I \otimes \sigma_z, \tau_x \otimes I, \tau_x \otimes \sigma_x, \tau_x \otimes \sigma_y, \tau_x \otimes \sigma_z, \tau_y \otimes I, \tau_y \otimes \sigma_x, \tau_y \otimes \sigma_y, \tau_y \otimes \sigma_z, \tau_z \otimes I, \tau_z \otimes \sigma_x, \tau_z \otimes \sigma_y, \tau_z \otimes \sigma_z\}$, which span the space of the four-by-four Hermitian matrices. If we arrange those 16 matrices successively in a single column, denoted by Γ, the problem reduces to search solutions of a set of 16 linear differential equations:

$$\partial_t \Gamma = \frac{2}{\hbar}\left(M + \frac{eEt}{\hbar} M_t\right)\Gamma, \quad (8)$$

where the concrete expressions of M and M_t are given in the Appendix.

Expanding Γ in series of the electric field, namely, $\Gamma = \Gamma^{(0)} + \Gamma^{(1)} + \cdots$, we have the following equations:

$$\partial_t \Gamma^{(0)} = \frac{2}{\hbar} M \Gamma^{(0)},$$

$$\partial_t \Gamma^{(1)} = \frac{2}{\hbar} M \Gamma^{(1)} + \frac{2eEt}{\hbar^2} M_t \Gamma^{(0)}, \quad (9)$$

up to the first order. Using the standard method to solve these equations, we obtain the linear order term $I \otimes \sigma_z^{(1)}$ in the limit $t \to 0$:

$$I \otimes \sigma_z^{(1)} = \frac{eE}{2k(\beta^2 + \alpha\_^2 k^2 - \alpha_+^2 k^2)} \times (C_1 I \otimes \sigma_{0x} + C_2 I \otimes \sigma_{0y} + C_3 \tau_z \otimes \sigma_{0x} + C_4 \tau_z \otimes \sigma_{0y}), \quad (10)$$

where σ_{0a} stand for the initial values of σ_a at $t=0$ and the coefficients C are written out in the Appendix. The spin currents in both layers produced by the states in each energy band are evaluated as

$$\langle \psi_{1,f} | \hat{j}_y^z | \psi_{1,f} \rangle = eE\hbar^2 \sin^2\varphi \times \frac{(\sqrt{\beta^2 + \alpha\_^2 k^2} - \alpha\_ k)[\beta^2 - (\alpha_+^2 - \alpha_+\alpha\_)k^2]}{8m\alpha_+ k\sqrt{\beta^2 + \alpha\_^2 k^2}[\beta^2 - (\alpha_+^2 - \alpha\_^2)k^2]},$$

$$\langle \psi_{3,f} | \hat{j}_y^z | \psi_{3,f} \rangle = -eE\hbar^2 \sin^2\varphi \times \frac{(\sqrt{\beta^2 + \alpha\_^2 k^2} + \alpha\_ k)[\beta^2 - (\alpha_+^2 - \alpha_+\alpha\_)k^2]}{8m\alpha_+ k\sqrt{\beta^2 + \alpha\_^2 k^2}[\beta^2 - (\alpha_+^2 - \alpha\_^2)k^2]},$$

$$\langle \psi_{1,b} | \hat{j}_y^z | \psi_{1,b} \rangle = -eE\hbar^2 \sin^2\varphi \times \frac{(\sqrt{\beta^2 + \alpha\_^2 k^2} + \alpha\_ k)[(\alpha_+^2 + \alpha_+\alpha\_)k^2 - \beta^2]}{8m\alpha_+ k\sqrt{\beta^2 + \alpha\_^2 k^2}[\beta^2 - (\alpha_+^2 - \alpha\_^2)k^2]},$$

$$\langle \psi_{3,b} | \hat{j}_y^z | \psi_{3,b} \rangle = eE\hbar^2 \sin^2\varphi \times \frac{(\sqrt{\beta^2 + \alpha\_^2 k^2} - \alpha\_ k)[(\alpha_+^2 + \alpha_+\alpha\_)k^2 - \beta^2]}{8m\alpha_+ k\sqrt{\beta^2 + \alpha\_^2 k^2}[\beta^2 - (\alpha_+^2 - \alpha\_^2)k^2]},$$

while

$$\langle \psi_{2,f(b)} | \hat{j}_y^z | \psi_{2,f(b)} \rangle = -\langle \psi_{1,f(b)} | \hat{j}_y^z | \psi_{1,f(b)} \rangle,$$

$$\langle \psi_{4,f(b)} | \hat{j}_y^z | \psi_{4,f(b)} \rangle = -\langle \psi_{3,f(b)} | \hat{j}_y^z | \psi_{3,f(b)} \rangle. \quad (11)$$

The total spin current in each layer is the sum of the contributions of the four bands up to the Fermi level, i.e., $J_{f(b)y}^z = \sum_{j,k} \langle \psi_{j,f(b)} | \hat{j}_y^z | \psi_{j,f(b)} \rangle n_F(\varepsilon_j)/(L_x \times L_y)$, where $n_F(\varepsilon_j)$ is the Fermi distribution function and $L_x \times L_y$ the size of the system. The explicit expressions for $J_{f(b)y}^z$ at zero temperature are given in the Appendix. Equation (11) tells us that the spin currents produced by the states in bands ε_1 and ε_2 are always with the opposite sign. Thus only the contributions by the states in ε_2 with momentum $k_{F1} < k < k_{F2}$ remain. The case for bands ε_3 and ε_4 is similar. Here and throughout the paper, k_{Fj} denotes the Fermi wave vector in the band ε_j.

The full spin current of the whole bilayer system is given by $J_y^z = J_{fy}^z + J_{by}^z$ and the corresponding spin Hall conductivity

is defined as $\sigma_s = \partial J_y^z / \partial E$. Our results can also be verified by Kubo formula. It is worthwhile to observe our results in two specific cases. In the case that the tunneling is absent, the system becomes a decoupled two single layers and its spin Hall conductivity becomes $\sigma_s = e/4\pi$, twice of the universal value in a single layer.[6] In the case of $\alpha_- \to 0$, there is no difference between the two layers and thus they cannot be distinguished. Consequently, no matter the tunneling is present or not, they behave just like decoupled two single layers since tunneling to the other layer makes no difference from staying in the original one.

Now we are in the position to investigate the tunneling dependence of spin Hall conductivities σ_f and σ_b in each layer. Based on the above results, we plot σ_f, σ_b as well as σ_s in Fig. 2. The dependence of the spin Hall conductivity in each layer on the strength of the SOC is quite different from that in a single-layer system which does not vary as the strength of the SOC changes. As illustrated in Fig. 2(a), $\sigma_{f(b)}$ increases (decreases) monotonously as the strength of the SOC in its layer increases (decreases) while σ_s keeps constant. We also plot σ_f and σ_b versus the tunneling strength in Fig. 2(b) and 2(c). They change abruptly near β_t where $k_{F1} = k_{F2} = k_t$ and also undergo sign changes across this point. At this point, the spin current produced by the states in band ε_1 and that in band ε_2 cancels each other precisely, leading to a depression of σ_s which always keeps a constant value $e/4\pi$ for $\beta \neq \beta_t$. It manifests that each layer possesses a large spin conductivity near β_t, while σ_s of the whole system remains $e/4\pi$. These features are instructive for designing experiments to detect a magnified spin Hall effect.

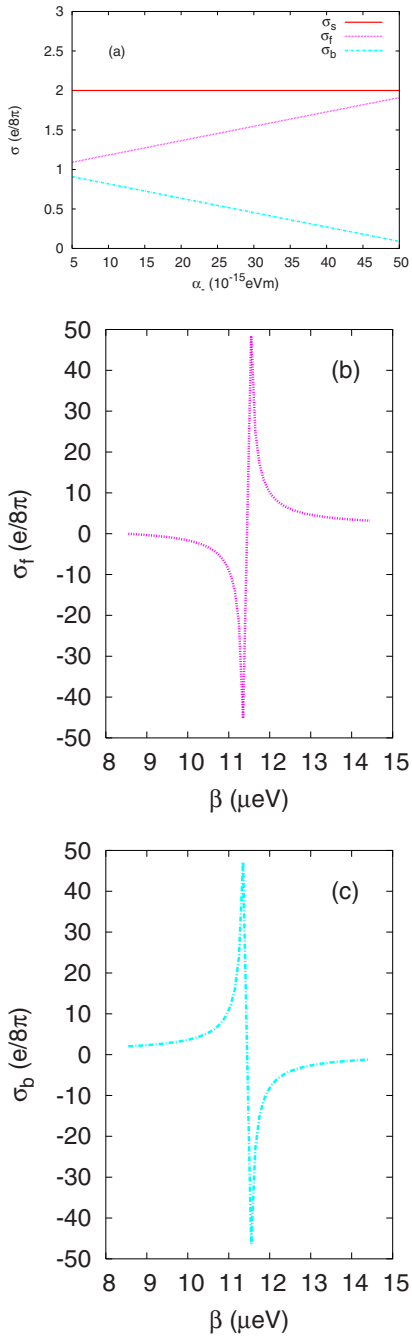

FIG. 2. (Color online) (a) Spin currents in each layer and in the whole system versus α_- are plotted with $\alpha_+ = 0.55 \times 10^{-13}$ eV m and $\beta = 4.013 \times 10^{-4}$ eV. [(b) and (c)] Spin currents in each layer versus the tunneling strength β are plotted with $\alpha_1 = 10^{-13}$ eV m and $\alpha_2 = 10^{-14}$ eV m, in which sharp peaks emerge near β_t. The choices of the other parameters in the above figures: the Fermi energy $\varepsilon_F = 0.1$ eV and the effective mass $m = 0.05 m_e$.

IV. IMPURITY EFFECTS

In realistic systems, disorderly distributed impurities are unavoidable, which frequently affect transport properties. It was believed that the spin Hall conductivity in a single layer electron gas could be suppressed to zero by the vertex corrections of nonmagnetic impurities even for an infinitesimally small concentration.[7–11] Therefore, it is necessary to investigate the impurity effects in the bilayer system.

We consider disorderly deployed nonmagnetic impurities. The short-ranged interaction between the electron and impurities at positions R_i is described by $\hat{V}_{\text{im}} = \Sigma_i u \delta(r - R_i)$. Here we assume the coupling strength u is sufficiently weak so that the Born approximation is applicable. The averaged retarded Green's function satisfies the Dyson equation $\bar{G}^R = G_0^R + G_0^R \bar{\Sigma}^R \bar{G}^R$ where the overbar, refers to an average taken over the configuration of impurities, G_0^R denotes the free Green's function, and Σ^R the self-energy brought about by the impurities. In the Born approximation,[21] the Dyson equation can be explicitly written as

$$\bar{G}^R(\vec{p},\omega) = G_0^R(\vec{p},\omega) + G_0^R(\vec{p},\omega) \times \left(u n_{\text{im}} + \frac{u^2 n_{\text{im}}}{\nu} \sum_{\vec{q}} \bar{G}^R(\vec{q},\omega) \right) \bar{G}^R(\vec{p},\omega), \tag{12}$$

where n_{im} stands for the impurity concentration and ν the size of the whole system.

For convenience, we introduce the chiral representation in which the H_0 is diagonalized by a unitary matrix U, i.e., $U^\dagger H_0 U = \text{diag}(\varepsilon_1, \varepsilon_2, \varepsilon_3, \varepsilon_4)$. In this representation, the free retarded Green's function reads $G_{0(ch)}^R(\vec{p},\omega) = \text{diag}((\omega - \varepsilon_1 + i\eta)^{-1}, (\omega - \varepsilon_2 + i\eta)^{-1}, (\omega - \varepsilon_3 + i\eta)^{-1}, (\omega - \varepsilon_4 + i\eta)^{-1})$ such that Eq. (12) solves

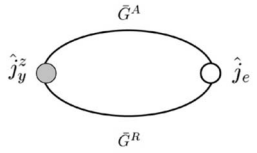

FIG. 3. One-loop diagram which contributes to $\bar{\sigma}_s^0$.

$$\bar{G}^R_{(ch)}(\vec{p},\omega)=\begin{pmatrix} g_1 & 0 & 0 & 0 \\ 0 & g_2 & 0 & 0 \\ 0 & 0 & g_3 & 0 \\ 0 & 0 & 0 & g_4 \end{pmatrix},$$

with $g_j=1/\left(\omega-\varepsilon_j+\frac{i}{2\tau}\right)$ for $j=1,\ldots,4$. Here $\tau=(2\pi u^2 n_{\rm im}N_F)^{-1}$ is the momentum-relaxation time and N_F the density of states of the electron at the Fermi surface.

In terms of the Kubo formula, the averaged spin Hall conductivity at zero temperature can be calculated,

$$\bar{\sigma}_s(\omega)=\frac{e}{\omega\nu}\int\frac{d\omega'}{2\pi}\mathrm{Tr}\{\theta(-\omega'-\omega)\overline{\times\hat{j}_y^z[G^R(\omega'+\omega)-G^A(\omega'+\omega)]\hat{j}_e G^A(\omega')}+\theta(-\omega')\overline{\hat{j}_y^z G^R(\omega'+\omega)\hat{j}_e[G^R(\omega')-G^A(\omega')]}\},\tag{13}$$

where G^A is the advanced Green's function, $\hat{j}_e=e\hat{v}_x$ the charge-current operator, and $\theta(\omega)$ the step function representing the Fermi distribution function at zero temperature. The trace Tr in Eq. (13) implies both the conventional trace over the spin indices and the summation over the momenta. In the uncrossing approximation,[10] $\bar{\sigma}_s$ is the sum of $\bar{\sigma}_s^0$ and $\bar{\sigma}_s^L$, the former is the contribution by one-loop diagram (shown in Fig. 3), while the latter is that by a series of ladder diagrams (shown in Fig. 4).

A. One-loop diagram contribution

To derive the dc conductivity, we take the limit $\omega\to 0$ in Eq. (14) and obtain the one-loop diagram contribution

$$\bar{\sigma}_s^0=\frac{e}{2\pi\nu}\mathrm{Tr}[\hat{j}_y^z(\vec{p})\bar{G}^R(\vec{p})\hat{j}_e(\vec{p})\bar{G}^A(\vec{p})]=\frac{e}{8\pi}\left[\chi^2\left(1-\frac{1}{1+\Delta_{12}^2\tau^2}+1-\frac{1}{1+\Delta_{34}^2\tau^2}\right)+2(1-\chi^2)\left(1-\frac{1}{1+\Delta_{13}^2\tau^2}\right)\right],\tag{14}$$

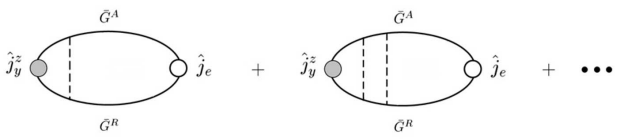

FIG. 4. The sum of the ladder diagrams gives the vertex correction to the spin Hall conductivity.

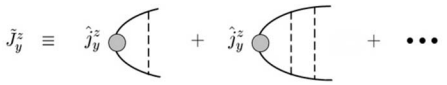

FIG. 5. The vertex $\tilde{J}_y^z$ is the sum of the vertex corrections to $\hat{j}_y^z(\vec{q})$.

where $\chi=\frac{\alpha_-\Delta_{13}}{\alpha_+\Delta_{14}}$ is a function of $\beta/(\alpha_- k_F)$. $\Delta_{ij}\equiv\varepsilon_i(k_F)-\varepsilon_j(k_F)$ is the energy splitting between two bands at the Fermi surface. The Fermi wave vector k_F is given by $\sqrt{2m\mu/\hbar}$ with μ being the chemical potential. In carrying out the summation of momentum in Eq. (14), we have adopted the large Fermi-circle limit $\mu\gg 1/\tau,\Delta_{ij}$.

Our result in Eq. (14) seems to be similar to the expression of a single layer system, $\bar{\sigma}_{sH}^0=\frac{e}{8\pi}\left(1-\frac{1}{1+\Delta^2\tau^2}\right)$. Moreover, the extra term in the last line of Eq. (14) and the prefactors χ^2 are peculiar in the bilayer system. It is worthwhile to observe the aforementioned two specific cases. In the case of zero tunneling $\beta\to 0$ ($\chi=-1$), we have $\bar{\sigma}_s^0=\frac{e}{8\pi}\left(1-\frac{1}{1+\Delta_f^2\tau^2}+1-\frac{1}{1+\Delta_b^2\tau^2}\right)$, where $\Delta_f=2\alpha_1 k_F$ and $\Delta_b=2\alpha_2 k_F$ are the spin-orbit splittings in each layer. It demonstrates that the system reduces to a decoupled one. In the twin-layer case $\alpha_-\to 0$ ($\chi=0$), we have $\bar{\sigma}_s^0=\frac{e}{4\pi}\left(1-\frac{1}{1+\Delta^2\tau^2}\right)$, which is just twice of the value of a single layer system. This is actually a trivial case as there is no difference between layers even though the tunneling is present. The above reasonable conclusions are consistent with the results for the clean system derived in previous section.

B. Vertex correction

The sum of ladder diagrams in Fig. 4 gives rise to $\bar{\sigma}_s^L$. By introducing a matrix-valued vertex $\tilde{J}_y^z$ which is the sum of the vertex correction to $\hat{j}_y^z$, as shown in Fig. 5, $\bar{\sigma}_s^L$ can be written as

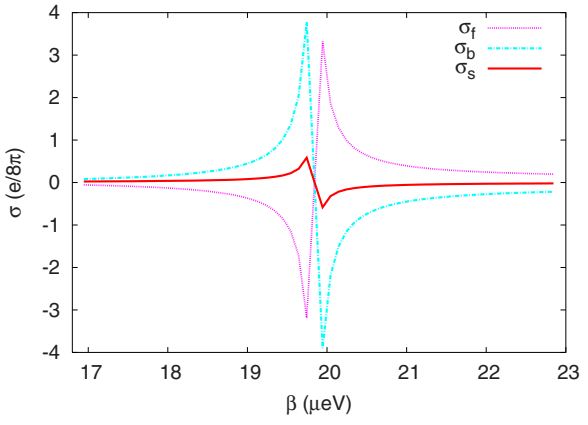

FIG. 6. (Color online) Spin conductivities for each layer $\bar{\sigma}_{f(b)}$ and the whole system $\bar{\sigma}_s$ are plotted with parameters $\alpha_+=0.55\times 10^{-13}$ eV m, $\alpha_-=0.45\times 10^{-14}$ eV m, and $\tau=6.6$ ns. Sharp cusps show up around the turning point β_t.

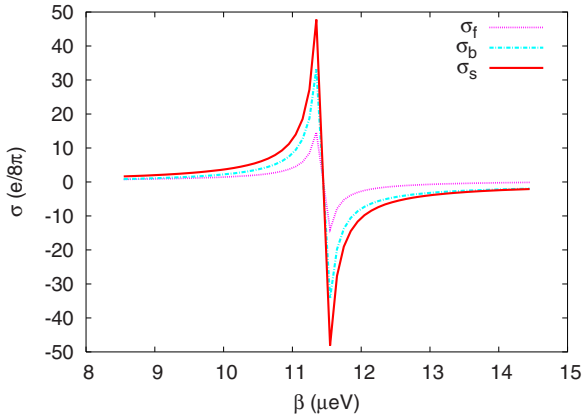

FIG. 7. (Color online) Spin conductivities in each layer $\bar{\sigma}_{f(b)}$ and the whole system $\bar{\sigma}_s$ are plotted with parameters $\alpha_+=0.55\times10^{-13}$ eV m, $\alpha_-=0.45\times10^{-13}$ eV m, and $\tau=6.6$ ns. The peak values of the conductivity in each layer is quite large and possesses the same sign.

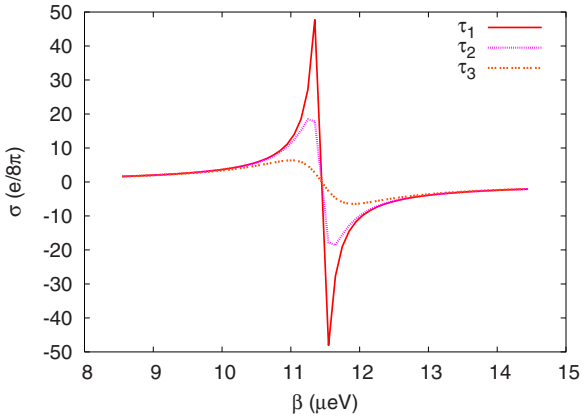

FIG. 8. (Color online) Spin conductivities for the whole system $\bar{\sigma}_s$ are plotted with different momentum-relaxation times: $\tau_1=6.6$ ns, $\tau_2=2.1$ ns, $\tau_3=0.66$ ns. Other parameters are the same as those in Fig. 7.

$$\bar{\sigma}_s^L=\frac{e}{2\pi\nu}\mathrm{Tr}[\tilde{J}_y^z\bar{G}^R(\vec{p})\hat{j}_e(\vec{p})\bar{G}^A(\vec{p})], \tag{15}$$

where $\tilde{J}_y^z$ is momentum independent and satisfies the transfer matrix equation

$$\tilde{J}_y^z=\frac{u^2n_{\mathrm{im}}}{\nu}\sum_{\vec{q}}\bar{G}^A(\vec{q})(\hat{j}_y^z(\vec{q})+\tilde{J}_y^z)\bar{G}^R(\vec{q}). \tag{16}$$

As a result, we have

$$\begin{aligned}\bar{\sigma}_s^L=\frac{e}{8\pi}\frac{\Delta_{13}\tau}{v_F}\Bigg\{&\left(2-\frac{\chi^2+\alpha_-\chi/\alpha_+}{1+\Delta_{12}^2\tau^2}-\frac{\chi^2-\alpha_+\chi/\alpha_+}{1+\Delta_{34}^2\tau^2}\right.\\&\left.-\frac{2(1-\chi^2)}{1+\Delta_{13}^2\tau^2}\right)i(J_{12}+J_{34})+\frac{\alpha_-}{\alpha_+}\left(2-\frac{1+\alpha_+\chi/\alpha_-}{1+\Delta_{12}^2\tau^2}\right.\\&\left.-\frac{1-\alpha_+\chi/\alpha_-}{1+\Delta_{34}^2\tau^2}-\frac{2(1-\chi^2)}{1+\Delta_{14}^2\tau^2}\right)i(J_{12}-J_{34})\\&-\frac{2\alpha_-\sqrt{1-\chi^2}\tau}{\alpha_+}\left[\frac{\Delta_{12}}{1+\Delta_{12}^2\tau^2}\left(1+\frac{\Delta_{13}}{\Delta_{14}}\right)+\frac{\Delta_{34}}{1+\Delta_{34}^2\tau^2}\right.\\&\left.\times\left(1-\frac{\Delta_{13}}{\Delta_{14}}\right)+\frac{2\Delta_{14}}{1+\Delta_{14}^2\tau^2}-\frac{\Delta_{13}}{\Delta_{14}}\frac{2\Delta_{13}}{1+\Delta_{13}^2\tau^2}\right]J_{14}\Bigg\}.\end{aligned} \tag{17}$$

where J_{12},J_{14},J_{34} are the matrix elements of $\tilde{J}_y^z$. Their explicit expressions, a solution of Eq. (16), are given in Eq. (A7) in the Appendix. When the tunneling vanishes, we have $\bar{\sigma}_s^L=-\frac{e}{8\pi}\left(1-\frac{1}{1+\Delta_f^2\tau^2}+1-\frac{1}{1+\Delta_b^2\tau^2}\right)$, reducing to the case of a decoupled bilayer system, and $\bar{\sigma}_s^L$ precisely cancels $\bar{\sigma}_s^0$, leading to a vanishing spin Hall conductivity. The nontrivial situation is that both the tunneling β and the difference in Rashba strength α_- are present, which makes $\bar{\sigma}_s$ survives.

V. MAGNIFICATION EFFECT AND POSSIBLE EXPERIMENTS

The spin Hall conductivity is the sum of $\bar{\sigma}_s^0$ and $\bar{\sigma}_s^L$. An arbitrarily small concentration of nonmagnetic impurities cannot suppress the spin Hall conductivity in a bilayer system to zero, which is quite different from the case in the single layer system. In Fig. 6, we plot the spin Hall conductivities for each layer $\bar{\sigma}_{f(b)}$ and for the whole system $\bar{\sigma}_s$ with $\alpha_+=0.55\times10^{-13}$ eV m and $\alpha_-=0.45\times10^{-14}$ eV m (i.e., the strength of the Rashba spin-orbit coupling in each layer are of the same order). The curves for the conductivities exhibit similar cusps around the turning point β_t as in Fig. 2 without impurities. The conductivity in each layer possesses opposite signs, leading to a quite small $\bar{\sigma}_s$ for the whole system. However, things are changed when α_- is comparably large. Figure 7 shows the conductivities with parameters $\alpha_+=0.55\times10^{-13}$ eV m and $\alpha_-=0.45\times10^{-13}$ eV m, i.e., the Rashba strength in the front layer is ten times as much as that in the back layer. The opposite signs of the conductivities in each layer in the absence of impurities turn to be the same in the presence of impurities. As a result, the peak value of $\bar{\sigma}_s$ for the whole system is considerably large. It suggests that a large difference in the strength of Rashba spin-orbit coupling between layers is favorable for a greatly enhanced spin Hall conductivity.

Above results are obtained with rather dilute impurities which requires the mobility of the two-dimensional electron gas to be quite high. The influence of the concentration of impurities on the spin Hall conductivities is also studied, as shown in Fig. 8. Increasing the concentration of impurities, we find that the peak value decreases. Although the impurities tend to suppress the spin Hall conductivity, $\bar{\sigma}_s$ would still be detectable. For a two-dimensional electron gas with its mobility of order 10^6 cm^2/V s which is in an experimentally realizable regime, the peak value of $\bar{\sigma}_s$ is around $e/8\pi$. Thus, the spin Hall conductivity for a bilayer electron system does not vanish and is expected to be measured in samples with high mobility.

We discuss possible experiments to detect the magnification of the spin Hall effect. Our proposal is based on the fact

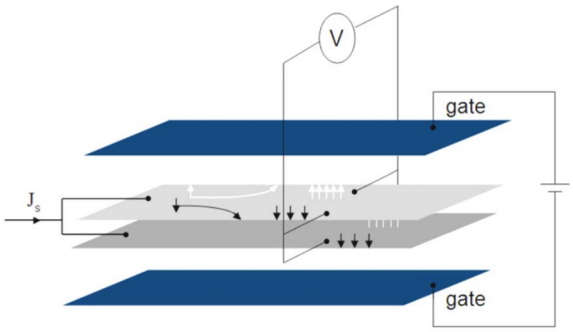

FIG. 9. (Color online) A proposed experimental scheme to detect a magnification of the spin Hall effect. By injecting spin current (charge current with spin mostly polarized) into a bilayer spin Hall bar and connecting the voltmeter to measure the transverse voltage, a greatly enhanced Hall voltage is expected to be observed near the turning point β_t.

that a spin-polarized electric current (means the existence of spin current) in the presence of the SOC can induce different charge populations at the laterals and hence a Hall voltage can be detected.[18] Since the induced Hall voltage is in proportional to the spin Hall conductivity, its magnitude is greatly enhanced near the turning point β_t in the coupled bilayer electron gas. As the tunneling strength can be tuned by the gate voltage, we therefore suggest experimentally detect an enormously magnified Hall voltage by tuning the tunneling strength to be near β_t in the bilayer system (see Fig. 9). Additionally, the sign changes of spin Hall conductivity across β_t also make the coupled bilayer system a candidate for fabricating possible logical gates.

VI. SUMMARY

We investigated the properties of the spin transport in a coupled bilayer system where the strength of the SOC in each layer may be different and the tunneling between the two layers occurs. We gave natural definitions of the spin density and the spin current density in each layer and derived the corresponding "continuitylike" equations. Based on the calculations in Heisenberg representation, we obtained the spin current. The curves of the spin Hall conductivities in each layer exhibit sharp cusps around the turning point and the peak values have signs changed across this point. We also investigated the influence of impurities on the spin Hall conductivity. We found that an arbitrarily small concentration of nonmagnetic impurities does not suppress the spin Hall conductivity to zero in a bilayer system, which is quite different from the case in the single layer system. The opposite signs of the conductivities in the absence of impurities become the same in the presence of impurities. Making use of these features, we proposed a possible experiment to detect a magnified spin Hall effect by direct electronic measurement. The sign-change property may also be used in designing certain logical gates.

ACKNOWLEDGMENT

The work was supported by NSFC Grant Nos. 10225419 and 10674117.

APPENDIX: EXPRESSIONS FOR SOME COEFFICIENTS AND THE MATRICES

The coefficient matrices in the linear Eq. (8) are written as

$$M = \begin{pmatrix}
0 & 0 & 0 & 0 & 0 & 0 & 0 & 0 & 0 & 0 & 0 & 0 & 0 & 0 & 0 & 0 \\
0 & 0 & 0 & -f_x^+ & 0 & 0 & 0 & 0 & 0 & 0 & 0 & 0 & 0 & 0 & 0 & -f_x^- \\
0 & 0 & 0 & -f_y^+ & 0 & 0 & 0 & 0 & 0 & 0 & 0 & 0 & 0 & 0 & 0 & -f_y^- \\
0 & f_x^+ & f_y^+ & 0 & 0 & 0 & 0 & 0 & 0 & 0 & 0 & 0 & 0 & f_x^- & f_y^- & 0 \\
0 & 0 & 0 & 0 & 0 & 0 & 0 & 0 & 0 & -f_y^- & f_x^- & 0 & 0 & 0 & 0 & 0 \\
0 & 0 & 0 & 0 & 0 & 0 & 0 & -f_x^+ & -f_y^- & 0 & 0 & 0 & 0 & 0 & 0 & 0 \\
0 & 0 & 0 & 0 & 0 & 0 & 0 & -f_y^+ & f_x^- & 0 & 0 & 0 & 0 & 0 & 0 & 0 \\
0 & 0 & 0 & 0 & 0 & f_x^+ & f_y^+ & 0 & 0 & 0 & 0 & 0 & 0 & 0 & 0 & 0 \\
0 & 0 & 0 & 0 & 0 & f_y^- & -f_x^- & 0 & 0 & 0 & 0 & 0 & -\beta & 0 & 0 & 0 \\
0 & 0 & 0 & 0 & f_y^- & 0 & 0 & 0 & 0 & 0 & 0 & -f_x^+ & 0 & -\beta & 0 & 0 \\
0 & 0 & 0 & 0 & -f_x^- & 0 & 0 & 0 & 0 & 0 & 0 & -f_y^+ & 0 & 0 & -\beta & 0 \\
0 & 0 & 0 & 0 & 0 & 0 & 0 & 0 & 0 & f_x^+ & f_y^+ & 0 & 0 & 0 & 0 & -\beta \\
0 & 0 & 0 & 0 & 0 & 0 & 0 & 0 & \beta & 0 & 0 & 0 & 0 & 0 & 0 & 0 \\
0 & 0 & 0 & -f_x^- & 0 & 0 & 0 & 0 & 0 & \beta & 0 & 0 & 0 & 0 & 0 & -f_x^+ \\
0 & 0 & 0 & -f_y^- & 0 & 0 & 0 & 0 & 0 & 0 & \beta & 0 & 0 & 0 & 0 & -f_y^+ \\
0 & f_x^- & f_y^- & 0 & 0 & 0 & 0 & 0 & 0 & 0 & 0 & \beta & 0 & f_x^+ & f_y^+ & 0
\end{pmatrix}, \tag{A1}$$

where $f_x^\pm = \alpha_\pm k_{0x}$ and $f_y^\pm = \alpha_\pm k_{0y}$, and

$$M_t = \begin{pmatrix}
0 & 0 & 0 & 0 & 0 & 0 & 0 & 0 & 0 & 0 & 0 & 0 & 0 & 0 & 0 & 0 \\
0 & 0 & 0 & \alpha_+ & 0 & 0 & 0 & 0 & 0 & 0 & 0 & 0 & 0 & 0 & 0 & \alpha_- \\
0 & 0 & 0 & 0 & 0 & 0 & 0 & 0 & 0 & 0 & 0 & 0 & 0 & 0 & 0 & 0 \\
0 & -\alpha_+ & 0 & 0 & 0 & 0 & 0 & 0 & 0 & 0 & 0 & 0 & 0 & -\alpha_- & 0 & 0 \\
0 & 0 & 0 & 0 & 0 & 0 & 0 & 0 & 0 & 0 & -\alpha_- & 0 & 0 & 0 & 0 & 0 \\
0 & 0 & 0 & 0 & 0 & 0 & 0 & \alpha_+ & 0 & 0 & 0 & 0 & 0 & 0 & 0 & 0 \\
0 & 0 & 0 & 0 & 0 & 0 & 0 & 0 & -\alpha_- & 0 & 0 & 0 & 0 & 0 & 0 & 0 \\
0 & 0 & 0 & 0 & 0 & -\alpha_+ & 0 & 0 & 0 & 0 & 0 & 0 & 0 & 0 & 0 & 0 \\
0 & 0 & 0 & 0 & 0 & 0 & \alpha_- & 0 & 0 & 0 & 0 & 0 & 0 & 0 & 0 & 0 \\
0 & 0 & 0 & 0 & 0 & 0 & 0 & 0 & 0 & 0 & 0 & \alpha_+ & 0 & 0 & 0 & 0 \\
0 & 0 & 0 & 0 & \alpha_- & 0 & 0 & 0 & 0 & 0 & 0 & 0 & 0 & 0 & 0 & 0 \\
0 & 0 & 0 & 0 & 0 & 0 & 0 & 0 & 0 & -\alpha_+ & 0 & 0 & 0 & 0 & 0 & 0 \\
0 & 0 & 0 & 0 & 0 & 0 & 0 & 0 & 0 & 0 & 0 & 0 & 0 & 0 & 0 & 0 \\
0 & 0 & 0 & \alpha_- & 0 & 0 & 0 & 0 & 0 & 0 & 0 & 0 & 0 & 0 & 0 & \alpha_+ \\
0 & 0 & 0 & 0 & 0 & 0 & 0 & 0 & 0 & 0 & 0 & 0 & 0 & 0 & 0 & 0 \\
0 & -\alpha_- & 0 & 0 & 0 & 0 & 0 & 0 & 0 & 0 & 0 & 0 & 0 & -\alpha_+ & 0 & 0
\end{pmatrix}. \tag{A2}$$

The normalization coefficients for the eigenvectors in Eq. (6) read

$$N_1 = \frac{1}{2}[\beta^2 + \alpha_-^2 k^2 - \alpha_- k\sqrt{\beta^2 + \alpha_-^2 k^2}]^{-1/2},$$

$$N_2 = \frac{1}{2\beta}[1 + \alpha_- k/\sqrt{\beta^2 + \alpha_-^2 k^2}]^{1/2},$$

$$N_3 = \frac{1}{2}[\beta^2 + \alpha_-^2 k^2 + \alpha_- k\sqrt{\beta^2 + \alpha_-^2 k^2}]^{-1/2},$$

$$N_4 = \frac{1}{2\beta}[1 - \alpha_- k/\sqrt{\beta^2 + \alpha_-^2 k^2}]^{1/2}. \tag{A3}$$

The coefficients in the Eq. (10) are written as

$$C_1 = -\frac{(\beta^2 - \alpha_+^2 k^2)\sin^2\varphi}{\alpha_+ k},$$

$$C_2 = \frac{(\beta^2 - \alpha_+^2 k^2)\sin\varphi\cos\varphi}{\alpha_+ k},$$

$$C_3 = \frac{\alpha_- k}{2(\beta^2 + \alpha_-^2 k^2)^2}[-2\beta^4 - 2\sin^2\varphi\alpha_-^4 k^4 + \beta^2(2\cos^2\varphi\alpha_+^2 + (\cos 2\varphi - 3)\alpha_-^2)k^2],$$

$$C_4 = \frac{\alpha_- k^3 \sin 2\varphi}{2(\beta^2 + \alpha_-^2 k^2)^2}[\beta^2(\alpha_-^2 + \alpha_+^2) + \alpha_-^4 k^2]. \tag{A4}$$

The total spin current for each layer in a realistic sample of size $L_x \times L_y$ is given by

$$J_{fy}^z = \frac{1}{L_x L_y}\sum_{i=1}^{4}\sum_k \psi_{i,f}^\dagger \hat{j}_y^z \psi_{i,f}$$
$$= \frac{\hbar^2 eE}{32\pi m\alpha_+(\alpha_+ + \alpha_-)}\left\{\left[\alpha_+ k - \frac{\alpha_+}{\alpha_-}\sqrt{\beta^2 + \alpha_-^2 k^2} - \frac{\alpha_-\beta}{2\sqrt{\alpha_+^2 - \alpha_-^2}}\left(\ln\left|\frac{\sqrt{\alpha_+^2 - \alpha_-^2}k - \beta}{\sqrt{\alpha_+^2 - \alpha_-^2}k + \beta}\right| - \frac{\alpha_-}{\alpha_+}\ln\left|\frac{\sqrt{\alpha_+^2 - \alpha_-^2}\sqrt{\beta^2 + \alpha_-^2 k^2} - \alpha_+\beta}{\sqrt{\alpha_+^2 - \alpha_-^2}\sqrt{\beta^2 + \alpha_-^2 k^2} + \alpha_+\beta}\right|\right)\right]_{k_{F2}}^{k_{F1}}\right.$$
$$\left. - \left[\alpha_+ k + \frac{\alpha_+}{\alpha_-}\sqrt{\beta^2 + \alpha_-^2 k^2} - \frac{\alpha_-\beta}{2\sqrt{\alpha_+^2 - \alpha_-^2}}\left(\ln\left|\frac{\sqrt{\alpha_+^2 - \alpha_-^2}k - \beta}{\sqrt{\alpha_+^2 - \alpha_-^2}k + \beta}\right| + \frac{\alpha_-}{\alpha_+}\ln\left|\frac{\sqrt{\alpha_+^2 - \alpha_-^2}\sqrt{\beta^2 + \alpha_-^2 k^2} - \alpha_+\beta}{\sqrt{\alpha_+^2 - \alpha_-^2}\sqrt{\beta^2 + \alpha_-^2 k^2} + \alpha_+\beta}\right|\right)\right]_{k_{F4}}^{k_{F3}}\right\},$$

$$J_{by}^{z} = \frac{1}{L_x L_y}\sum_{i=1}^{4}\sum_{k}\psi_{i,b}^{\dagger}\hat{J}_{y}^{z}\psi_{i,b}$$

$$= \frac{\hbar^2 eE}{32\pi m\alpha_+(\alpha_+ - \alpha_-)}\left\{\left[\alpha_+ k + \frac{\alpha_+}{\alpha_-}\sqrt{\beta^2 + \alpha_-^2 k^2} + \frac{\alpha_-\beta}{2\sqrt{\alpha_+^2 - \alpha_-^2}}\left(\ln\left|\frac{\sqrt{\alpha_+^2 - \alpha_-^2}k - \beta}{\sqrt{\alpha_+^2 - \alpha_-^2}k + \beta}\right| + \frac{\alpha_-}{\alpha_+}\ln\left|\frac{\sqrt{\alpha_+^2 - \alpha_-^2}\sqrt{\beta^2 + \alpha_-^2 k^2} - \alpha_+\beta}{\sqrt{\alpha_+^2 - \alpha_-^2}\sqrt{\beta^2 + \alpha_-^2 k^2} + \alpha_+\beta}\right|\right)\right]_{k_{F2}}^{k_{F1}}\right.$$

$$\left. - \left[\alpha_+ k - \frac{\alpha_+}{\alpha_-}\sqrt{\beta^2 + \alpha_-^2 k^2} + \frac{\alpha_-\beta}{2\sqrt{\alpha_+^2 - \alpha_-^2}}\left(\ln\left|\frac{\sqrt{\alpha_+^2 - \alpha_-^2}k - \beta}{\sqrt{\alpha_+^2 - \alpha_-^2}k + \beta}\right| - \frac{\alpha_-}{\alpha_+}\ln\left|\frac{\sqrt{\alpha_+^2 - \alpha_-^2}\sqrt{\beta^2 + \alpha_-^2 k^2} - \alpha_+\beta}{\sqrt{\alpha_+^2 - \alpha_-^2}\sqrt{\beta^2 + \alpha_-^2 k^2} + \alpha_+\beta}\right|\right)\right]_{k_{F4}}^{k_{F3}}\right\}. \quad \text{(A5)}$$

The above results are derived by assuming that the special point k_t is far away from the Fermi momenta. When $k_{F3} < k_t = k_{F1} = k_{F2} < k_{F4}$, the spin current produced by the state with k_t is given by $\hbar^2(2\alpha_+^2 - \alpha_-^2)/4m\alpha_+^3 k_t$ in unit of $eE/4\pi$.

The matrix elements J_{12}, J_{14}, J_{34} of $\tilde{J}_y^z$ can be solved from Eq. (16), which is, in fact, a task of solving a set of linear equations

$$\begin{pmatrix} w_+ & 2\lambda_+ & \tilde{w} \\ \lambda_+ & w_m & -\lambda_- \\ \tilde{w} & -2\lambda_- & w_- \end{pmatrix}\begin{pmatrix} J_{12} \\ J_{14} \\ J_{34} \end{pmatrix} = \begin{pmatrix} -q_+ \\ q_m \\ q_- \end{pmatrix}. \quad \text{(A6)}$$

The solutions are given by

$$J_{12} = \frac{1}{d}[q_+(w_- w_m - 2\lambda_-^2) + 2q_m(w_-\lambda_+ + \tilde{w}\lambda_-) - q_-(\tilde{w}w_m + 2\lambda_+\lambda_-)],$$

$$J_{14} = -\frac{1}{d}[q_+(w_-\lambda_+ + \tilde{w}\lambda_-) + q_m(w_+ w_- - \tilde{w}^2) - q_-(\tilde{w}\lambda_+ + w_+\lambda_-)],$$

$$J_{34} = -\frac{1}{d}[q_+(\tilde{w}w_m + 2\lambda_+\lambda_-) + 2q_m(w_+\lambda_- + \tilde{w}\lambda_+) - q_-(w_+ w_m - 2\lambda_+^2)], \quad \text{(A7)}$$

with coefficients

$$d = (\tilde{w}^2 - w_+ w_-)w_m + 2(w_-\lambda_+^2 + w_+\lambda_-^2 + 2\tilde{w}\lambda_+\lambda_-),$$

$$w_\pm = \frac{1}{4}\left[2 + (1-\chi^2)\left(1 - \frac{1}{1+\Delta_{13}^2\tau^2} - \frac{1}{1+\Delta_{14}^2\tau^2}\right) - \frac{\frac{1}{2}(\chi^2+1) \pm \chi}{1+\Delta_{12}^2\tau^2} - \frac{\frac{1}{2}(\chi^2+1) \mp \chi}{1+\Delta_{34}^2\tau^2}\right],$$

$$w_m = 1 - \frac{1}{2(1+\Delta_{14}^2\tau^2)} - \frac{1}{4}\left[\frac{2\chi^2}{1+\Delta_{13}^2\tau^2} + (1-\chi^2)\left(\frac{1}{1+\Delta_{12}^2\tau^2} + \frac{1}{1+\Delta_{34}^2\tau^2}\right)\right],$$

$$\tilde{w} = \frac{1-\chi^2}{8}\left[\frac{1}{1+\Delta_{12}^2\tau^2} + \frac{1}{1+\Delta_{34}^2\tau^2} - 2\left(1 + \frac{1}{1+\Delta_{13}^2\tau^2} - \frac{1}{1+\Delta_{14}^2\tau^2}\right)\right],$$

$$\lambda_\pm = \frac{i\sqrt{1-\chi^2}\tau}{8}\left[\frac{\Delta_{12}(1 \pm \chi)}{1+\Delta_{12}^2\tau^2} + \frac{\Delta_{34}(1 \mp \chi)}{1+\Delta_{34}^2\tau^2} \mp \frac{\chi\Delta_{13}}{1+\Delta_{13}^2\tau^2} + \frac{\Delta_{14}}{1+\Delta_{14}^2\tau^2}\right],$$

$$q_\pm = -\frac{iv_F\tau}{8}\left[\frac{\Delta_{12}(\chi^2 \pm \chi)}{1+\Delta_{12}^2\tau^2} - \frac{\Delta_{34}(\chi^2 \mp \chi)}{1+\Delta_{34}^2\tau^2} + \frac{2(1-\chi^2)\Delta_{13}}{1+\Delta_{13}^2\tau^2}\right],$$

$$q_m = -\frac{v_F\chi\sqrt{1-\chi^2}}{8}\left(\frac{1}{1+\Delta_{12}^2\tau^2} + \frac{1}{1+\Delta_{34}^2\tau^2} - \frac{2}{1+\Delta_{13}^2\tau^2}\right). \quad \text{(A8)}$$

where v_F is the Fermi velocity.

[1] M. I. Dyakonov and V. I. Perel, JETP Lett. **13**, 467 (1971).
[2] S. A. Wolf, D. D. Awschalom, R. A. Buhrman, J. M. Daughton, S. von Molnar, M. L. Roukes, A. Y. Chtchelkanova, and D. M. Tresger, Science **294**, 1488 (2001).
[3] I. Zutic, J. Fabian, and S. DasSarma, Rev. Mod. Phys. **76**, 323 (2004).
[4] J. E. Hirsch, Phys. Rev. Lett. **83**, 1834 (1999); M. I. Dyakonov and V. I. Perel, JETP Lett. **13**, 467 (1971).
[5] S. Murakami, N. Nagaosa, and S. C. Zhang, Science **301**, 1348 (2003); Phys. Rev. B **69**, 235206 (2004).
[6] J. Sinova, D. Culcer, Q. Niu, N. A. Sinitsyn, T. Jungwirth, and A. H. MacDonald, Phys. Rev. Lett. **92**, 126603 (2004).
[7] J. I. Inoue, G. E. W. Bauer, and L. W. Molenkamp, Phys. Rev. B **67**, 033104 (2003); *ibid.* **70**, 041303(R) (2004).
[8] E. G. Mishchenko, A. V. Shytov, and B. I. Halperin, Phys. Rev. Lett. **93**, 226602 (2004).
[9] R. Raimondi and P. Schwab, Phys. Rev. B **71**, 033311 (2005).
[10] Ol'ga V. Dimitrova, Phys. Rev. B **71**, 245327 (2005).
[11] H.-A. Engel, E. I. Rashba, and B. I. Halperin, *Handbook of Magnetism and Advanced Magnetic Materials* (Wiley, New York, 2006), Vol. V.
[12] J. I. Inoue, T. Kato, Y. Ishikawa, H. Itoh, G. E. W. Bauer, and L. W. Molenkamp, Phys. Rev. Lett. **97**, 046604 (2006).
[13] P. Wang, Y. Q. Li, and X. Zhao, Phys. Rev. B **75**, 075326 (2007).
[14] J. Wunderlich, B. Kästner, J. Sinova, and T. Jungwirth, Phys. Rev. Lett. **94**, 047204 (2005).
[15] Y. K. Kato, R. C. Myers, A. C. Gossard, and D. D. Awschalom, Nature (London) **427**, 50 (2004); Phys. Rev. Lett. **93**, 176601 (2004); Science **306**, 1910 (2004).
[16] V. Sih, W. H. Lau, R. C. Myers, V. R. Horowitz, A. C. Gossard, and D. D. Awschalom, Phys. Rev. Lett. **97**, 096605 (2006).
[17] H. Zhao, E. J. Loren, H. M. van Driel, and A. L. Smirl, Phys. Rev. Lett. **96**, 246601 (2006).
[18] S. O. Valenzuela and M. Tinkham, Nature (London) **442**, 176–179 (2006).
[19] P. Q. Jin, Y. Q. Li, and F. C. Zhang, J. Phys. A **39**, 7115 (2006).
[20] S. Q. Shen, Phys. Rev. B **70**, 081311(R) (2004).
[21] H. Haug and A.-P. Jauho, *Quantum Kinetics in Transport and Optics of Semiconductors* (Springer-Verlag, Berlin, 1996).